Spectral Multi-Dimensional Scaling using Biharmonic Distance

Jun Yang[1], Alexander Jesuorobo Obaseki[1] and Jim X Chen[2]

[1]School of Electronic and Information Engineering, Lanzhou Jiaotong University, Lanzhou, Gansu 730070, China
[2]Department of Computer Science, George Mason University, Fairfax, VA 22030-4444, U.S.A.

Abstract: The spectral property of the Laplace-Beltrami operator has become relevant in shape analysis. One of the numerous methods that employ the strength of Laplace-Beltrami operator eigen-properties in shape analysis is the spectral multidimensional scaling which maps the MDS problem into the eigenspace of its Laplace-Beltrami operator. Using the biharmonic distance we show a further reduction in the complexities of the canonical form of shapes making similarities and dissimilarities of isometric shapes more efficiently computed. With the theoretical sound biharmonic distance we embed the intrinsic property of a given shape into a Euclidean metric space. Utilizing the farthest-point sampling strategy to select a subset of sampled points, we combine the potency of the spectral multidimensional scaling with global awareness of the biharmonic distance operator to propose an approach which embeds canonical forms images that shows further "resemblance" between isometric shapes. Experimental result shows an efficient and effective approximation with both distinctive local features and yet a robust global property of both the model and probe shapes. In comparison to a recent state-of-the-art work, the proposed approach can achieve comparable or even better results and have practical computational efficiency as well.

1 INTRODUCTION

The problem of shape matching has become an important research problem and a fundamental task in a wide range of geometric applications including but not limited to computer vision (Vankaick et al., 2011), texture mapping (Sumner and Popovic, 2004), mesh deformation (Kreavoy et al., 2003), morphing (Alexa, 2002), and shape retrieval (Jain and Zhang, 2006).This problem can be defined as finding the (dis)similarities between objects represented by point clouds or triangle meshes, say two different poses of the same object. Such a problem can be reduced to establishing a correspondence between two set of the mesh vertices, that is to say establishing a meaningful mapping between them. This mapping is either between coarse sets of feature points selected on the meshes, or a dense continuous one that involve all points on the two shapes.

The basic question is finding an effective, yet accurate way to quantify the similarity between a given reference surface; "the model" and some other version (articulated) of the model; "the probe". An extrinsic property characterizes how a particular surface is immersed into the ambient (Euclidean) space and thus changes as the surface undergoes transformations. Such a metric is not ideal to capture distinction between shapes as they are significant disparities between the extrinsic attributes of a shape and its articulated version. A deformation that preserves the intrinsic structure of the surface is called an "isometry" (Bronstein et al., 2006).Thus defining a computable deformation-invariant measure of intrinsic similarity between the surfaces becomes the task at hand.

2 RELATED WORK

Manifold learning refers to the process of non-linear dimensionality reduction of data. When target space of reduction (embedding) is Euclidean the procedure is also known as flattening and the output is called "canonical forms" (CF). Multi-Dimensional Scaling (MDS) is a class of computationally efficient methods used for embedding a canonical form.

One of the earliest methods finds a uniform parameterization for convoluted surfaces that is usually a priori in a more general surface matching procedure (Schwartz et al. 1989). This result led to

emergence of many efficient flattening algorithms like in texture mapping (Zigelman et al., 2002), higher dimensional Euclidean space embedding (Elad and Kimmel, 2003) that captures the intrinsic geometric structure of isometric surfaces and a more generalized framework (Bronstein et al., 2006) that uses Gromov-Hausdroff distance (Gromov, 1981) to compute partial embedding distance for both full and partial surface matching. The key to using MDS algorithm for embedding is to obtain intrinsic representation of the underlying surface which is invariant to inelastic bending, and then interpolate this representation to embed the surface in a new ambient space such that the intrinsic geometry of the surface is translated into its extrinsic geometry in the new space. Conventionally, a set of inter-geodesic distance between pairs of all surface points is used as input. This approach though efficient, is computationally expensive as the complexity requirement in storing all pairwise distance is quadratic in the number of data points which is restrictive in shapes with substantial amount of vertices.

In the last decade, a major breakthrough in the eigenspace of the mesh Laplacian (Wolter et al., 2006) has been exploited in variety of forms. Isospectral properties of the eigenvectors know from linear algebra provided theoretical foundations that have been extended to correspondence between 3D surfaces. Jain et al. (Jain et al., 2011) transformed 3D meshes into the spectral domain, based on geodesic affinities, and then matched the spectral embeddings of the eigenvectors with respect to uniform scaling and rigid-body transformation. Kim et al. (Kim et al., 2011) approached the problem by blending a collection of weighted low dimensional conformal maps. The multi-scale geometry aware properties of the Laplace Beltrami operator (LBO) are utilized to infer and manipulate point-to-point maps between shapes (Ovsjanikov et al., 2012). Rustamov (Rustamov, 2007) introduced a deformation invariant representation of surfaces similar to canonical forms which is based on combining eigenvalues and eigenvectors of LBO instead of geodesic distance. A LBO decomposition method is exploited to construct diffusion maps (Coifman and Lafon, 2006). Descriptors like Heat kernel signature (Sun et al., 2009), wave kernel signature (Aubry et al., 2011) are all based on eigenfunctions of the LBO.

Similar to our approach, Aflalo et al. (Aflalo and Kimmel, 2013) extracted the spectral data from the LBO of pairwise geodesic distance of sampled points, and then embedded the data into a low-dimensional Euclidean space. Computed a small fraction of the pairwise distances that was projected onto the leading eigenfunctions of the LBO, thus, efficiently reduced both the time and space complexities of the flattening procedure. It seems that they overcame a great amount of complexities, however, the question of its reliance on geodesic distance which has weak "global–awareness" and significantly large topological sensitivity is a major drawback to this approach.

In this paper, we argue that biharmonic distance (Lipman et al., 2010) can serve as an efficient yet accurate distance operator. The measure of biharmonic distance on shapes are smooth functions, thus are well suited for compact spectral representation, and as such allow us to apply this theoretically sound distance operator in a spectral sense. Biharmonic distance is a metric structure that is related to diffusion distance and commute-time distance (Fouss et al., 2007; Yen et al., 2007) with a slight modification in the eigenvalue normalization. Our motivation to use this distance operator is based on the fact that it finds a good trade-off between local and global properties of the shape. Here, the eigenvalue normalization decays slow enough to get good local properties around source points and fast enough to be globally aware of shape in far areas.

3 COMPUTING BIHARMONIC DISTANCE

Biharmonic distance is a distance operator endowed with the fundamental properties required for shape analysis, such as isometric invariant, practically efficient, parameter-free, insensitive to noise and topology, etc.

Let us consider a Riemannian manifold M equipped with a metric G. The metric G induces a Laplace-Beltrami operator (LBO) denoted by Δ_G. The LBO is self-adjoint and defines a set of functions called eigenfunctions, denoted by ϕ_i, such that $\Delta\phi_i = \lambda_i\phi_i$, where λ_i is the eigenvalue associated with ϕ_i at vertex i.

Biharmonic distance operator is similar to diffusion distance and the commute-time distance, however there is slight modification on the eigenvalue normalization. This normalization is based on a kernel, which is Green's function of the biharmonic differential equation. In the continuous setting, the squared distance is defined

by using the eigenfunctions of the LBO (Lipman et al., 2010):

$$d_B(x,y)^2 = \sum_{i=1}^{\infty} \frac{(\phi_i(x) - \phi_i(y))^2}{\lambda_i^2} \qquad (1)$$

The quadratic normalization as shown in the Eq. (1) provides a good trade-off in the sense that it decays slow enough to get good local properties around the point and fast enough to be shape aware in distance areas. The trade-off is intimately related to the biharmonic equation. Expanding Eq. (1) we obtain:

$$d_B(x,y)^2 = \sum_{i=1}^{\infty} \frac{|\phi_i(x)|^2}{\lambda_i^2} + \sum_{i=1}^{\infty} \frac{|\phi_i(y)|^2}{\lambda_i^2} - 2\sum_{i=1}^{\infty} \frac{\phi_i(x)\phi_i(y)}{\lambda_i^2} \qquad (2)$$
$$= g_B(x,x) + g_B(y,y) - 2g_B(x,y)$$

Using the Green's function of the biharmonic operator:

$$g_B(x,y) = \sum_{k=1}^{\infty} \frac{\phi_i(x)\phi_i(y)}{\lambda_i^2} \qquad (3)$$

The above equation satisfies the relation

$$\Delta^2_{(x)} \int g_B(x,y)f(y)dy = f(x) \qquad (4)$$

for "smooth enough" f (Coifman and Lafon, 2006).

From Eq. (3), a discrete construction based on the discrete Green's function g_d of the Bi-Laplacian is derived from the well-known cotangent formula discretization of the Laplace-Beltrami differential operator on shapes (Grinspun et al., 2006; Meyer et al., 2003).

$$\Delta_i = \frac{1}{A_i} \sum_{j \in N_{ei(i)}} \left(\cot \alpha_{ij} + \cot \beta_{ij} \right) \left(u_i - u_j \right) \qquad (5)$$

where Δ_i, denotes the discrete Laplacian evaluated at vertex i (for $i = 1, 2, \cdots, N$, N is the number of vertices), A_i is the Voronoi area at i^{th} shape vertex (Grinspun et al., 2006) and angles α_{ij}, β_{ij} are the two angles supporting the edge connecting vertices i and j respectively.

Having discretized the Laplacian, the Green's function of the Bi-Laplacian, $g_d \in \mathbb{R}^{N \times N}$ is defined by discretizing the relation in Eq. (4) to obtain:

$$L_d^2 g_d A f = f \qquad (6)$$

where $f \in \mathbb{R}^{N \times 1}$ is an arbitrary vector in the image of L_d^2. (See (Meyer et al., 2003) for prove).

Finally, having obtained g_d, the biharmonic distance on the shape is defined from Eq. (3):

$$d_B\left(v_i, v_j\right)^2 = g_d(i,i) + g_d(j,j) - 2g_d(i,j) \qquad (7)$$

4 SPECTRAL MULTIDIMENSIONAL SCALING

Let us consider the shape correspondence problem that involves searching for the best point to point matching of two given shapes, *S* and *Q*. The earliest method of using multidimensional scaling (MDS) to compute such an assignment was proposed by (Elad and Kimmel, 2003). There, the pairwise geodesic distances between all points on a 3D shape was mapped to a simpler 3D Euclidean distance.

The spectral multidimensional scaling (Aflalo and Kimmel, 2013) uses the fact that point to point correspondence between two shapes induces a map between the natural eigenspaces of the shapes, thus, project the MDS problem into the data's spectral domain extracted from its Laplace-Beltrami operator. In this framework, truncated eigenfunctions were used to faithfully approximate correspondence between the shapes. We will go forward to briefly explain this approach.

Consider a manifold *M*, with n points $\{V_i\}$, *P* is a subset of $\{V_i\}$ such that $|P| = p_s \leq n$, and a smooth function f is defined on $V_P = \{V_p, p \in P\}$. Computing a smooth interpolation function requires firstly constructing a continuous function h such that $\tilde{f}(V_p) = f(V_p), \forall p \in P$. Then a smooth function measure the smoothness of such a function, say up to L_2 norm as $E_{smooth}(f) = \int_M^n \|\nabla f\|_2^2 da = \int_M^n \langle \Delta f, f \rangle da$.

The problem of smooth interpolation could be rewritten as $\min_{h: M \to \mathbb{R}} E_{smooth}(h) = $ s.t. $h(V_p) = f(V_p), \forall p \in P$. Then we have $\int_M^n \|\nabla f\|_2^2 da = \int_M^n \langle \Delta h, h \rangle da$. Thus the interpolation problem could be written as:

$$\min_{h: M \to \mathbb{R}} \int_M^n \langle \Delta h, h \rangle da \text{ s.t. } h(V_p) = f(V_p), \forall p \in P \quad (8)$$

In a discrete setting the problem in Eq. (8) above can be rewritten as

$$\min_x x^T W x \qquad \text{s.t.} \qquad B x = f \qquad (9)$$

There the matrix *B*, represents a projection on the basis vectors $e_p, \forall p \in P$, *W* is the conformal discrete Laplacian without the area normalization and f is the sampled vector $f(V_p)$. Their novel

technique was to introduce $\hat{f}$, the spectral projection of f (the eigenvectors of the LBO $\{\phi_i\}_{i=1}^k$) as $x = \hat{f} = \sum_{i=1}^{k} \langle f, \phi_i \rangle \phi_i = \Phi\alpha$, where $\Delta\phi_i = \lambda\phi_i$. Note that Φ represents the matrix of eigenfunctions whose i^{th} column is ϕ_i such that $\alpha_i = \langle f, \phi_i \rangle$. Thus Eq. (9) is approximated as

$$\min_{\alpha \in \mathbb{R}^k} \alpha^T \Phi^T W \Phi\alpha \quad \text{s.t.} \quad B\Phi\alpha = f \qquad (10)$$

Since $\Lambda = \Phi^T W \Phi$, where Λ is the diagonal matrix whose elements λ_{ii} are the corresponding eigenvalues of linear transformation of the LBO L_d. Substituting Λ and adding the constraint check in the target function the solution is rewritten as

$$\alpha = 2\mu \left(\Lambda + \mu\Phi^T B^T B\Phi \right)^{-1} + \Phi^T B^T f = Mf \quad (11)$$

The discretized smooth energy of the matrix D is given by

$$E_{smooth}(D) = trace(D^T W D A) + trace(DWD^T A) \quad (12)$$

While the spectral projection of D onto Φ, is denoted in matrix form by

$$D = \Phi\alpha\Phi^T \qquad (13)$$

Substituting D into Eq. (12) we obtain the smooth spectral interpolation as

$$\min_{\alpha \in \mathbb{R}^{k \times k}} trace(\alpha^T \Lambda\alpha) + trace(\alpha\Lambda\alpha^T) +$$
$$\mu \sum_{(i,j) \in I} \left\| \left(\Phi\alpha\Phi^T \right)_{ij} - D(V_i, V_j) \right\|_F^2 \qquad (14)$$

where $\| \bullet \|_F$ is the Frobenius norm, k is the number of eigenfunctions.

A less accurate but efficient way to obtain an approximation of the spectral interpolation matrix α is given as

$$\alpha = MFM^T \qquad (15)$$

This is obtained by interpolating the column vectors f and ϕ_i. Note in the above equation F is simply a matrix of the sample points V_i, V_j and M represents a matrix such that $\alpha = Mf$ from Eq. (11).

5 SPECTRAL MDS USING BIHARMONIC DISTANCE

Following the method of spectral multidimensional scaling, we apply biharmonic distance to compute

the canonical forms for non-rigid shapes. Given M, a metric space endowed with a metric $D : M \times M \rightarrow \mathbb{R}$, and $V = \{V_1, V_2, \cdots, V_n\}$ a finite set of elements in M, the multidimensional scaling of V in $\mathbb{R}^k$ involves finding a set of points $X = \{X_1, X_2, \cdots, X_n\}$ in $\mathbb{R}^k$ whose pairwise Euclidean distances $d(X_i, X_j) = \|X_i - X_j\|^2$ are as close as possible to $D(V_i, V_j)$ for all (i, j).

For such an embedding, a family of MDS known as classical scaling can be realized by the following minimization program $\min_X \left\| X^T X - \frac{1}{2} JDJ \right\|_F$, where D represents a matrix defined by $D_{ij} = D(V_i, V_j)^2$ and $J = I_n - \frac{1}{n} 1_n 1_n^T$, or $J_{ij} = \delta_{ij} - \frac{1}{n}$.

Using Classical scaling in Eq. (13), we find the first k singular vectors and values of the matrix $-\frac{1}{2} JDJ$.

We utilize the farthest-point sampling strategy to select a subset of p_s sampled points, with indices P of the data. Then we compute the biharmonic distance between every two points of the sampled data $d_B(v_i, v_j)^2 \in M \times M$, $(i, j) \in I = P \times P$. Since we have solved the LBO to compute the biharmonic distance as discussed in section 3, the LBO is not required to re-compute, we thus, use the same data to find k eigenfunctions in the eigenbasis Φ of the LBO. Using the biharmonic distance we show a further reduction in the complexity of the canonical form of the shapes making comparison between similar and dissimilar shapes more efficiently computed. Using Eq. (14) and (15) we extract the spectral interpolation matrix α from the computed biharmonic distance and the eigenbasis Φ.

An outline of the steps to solve the canonical form using biharmonic distance is shown in the algorithm below:

Step1: Compute P; a subset of p_s points sampled from M.

Step2: Compute the matrix D of squared biharmonic distances between every two points $(p_i, p_j), i \in P, j \in P$.

Step3: Compute the matrices Φ, Λ containing the kth eigenvectors and corresponding eigenvalues of the Laplace-Beltrami operator of M.

Step4: Compute the matrix α.

Step5: Compute the singular value decomposition of the nxk matrix $JQ=SUV^{\mathrm{T}}$, where $J = I_n - \frac{1}{n}1_n1_n^{\mathrm{T}}$.

Step6: Compute the eigendecomposition of the kxk matrix $UV^{\mathrm{T}}\alpha VU$, such that $UV^{\mathrm{T}}\alpha VU = W\psi W^{\mathrm{T}}$.

Step7: Compute the matrix $Q = SW\psi^{\frac{1}{2}}$, such that $QQ^{\mathrm{T}} = J\Phi\alpha\Phi J$.

Step8: Return the first d columns of the matrix Q, where d is the embedding dimension.

6 EXPERIMENTAL RESULTS AND DISCUSSION

In our evaluations and experiments, we utilized the TOSCA (Bronstein et al., 2009) and SPACE (Anguelov et al., 2004) shape databases for our shape comparison experiments. TOSCA has 80 meshes representing different classes of shapes, while SCAPE has 72 meshes representing a human body in different poses. All the meshes are fitted to scanner data with a common template, and thus they share the same mesh topology.

A qualitative evaluation of the canonical form is represented in the Figure 1 showing our embedding into canonical forms against that of spectral MDS (Aflalo and Kimmel, 2013) for wolf and gorilla shapes in various near-isometric positions. For both approaches we selected 100 eigenfunctions for the interpolation of the sampled points. The figure is represented row-wise original shape model, canonical forms of spectral MDS (Aflalo and Kimmel, 2013), canonical forms for our approach respectively. Clearly our method shows a more simplified canonical form and thus will produce more efficient and accurate rigid alignment.

Next, we evaluate the distortion of the embedding between two isometric shapes h: $S{\rightarrow}T$ with respect to a "ground truth" we used a method similar to (Kim et al., 2011). Here, we computed for every point, p, on S in the ground truth correspondence, the geodesic distance, $d_S\left(h(p),h_{true}(p)\right)$ between the smoothness function, $h(p)$ and its true correspondence, $h_{true}(p)$. The difference between the geodesic distance is added up in an error measure such that

$$Err\left(h,h_{true}\right) = \sum_{p\in S} d_S\left(h(p),h_{true}(p)\right) \qquad (16)$$

here $\left(h(p),h_{true}(p)\right)$ is normalized by the square root of the area of the manifold S.

We generated a table to examine the distribution of errors. Table 1 shows percentage correspondence as a function of geodesic error. That is, the data of varying geodesic error threshold, τ, between the model and probe $h(p),h_{true}(p)$ against the average percentage of points correspondence for which $d_S\left(h(p),h_{true}(p)\right)\leq\tau$. Taking an instance from the "animal shapes" in Table 1, about 67% of sample points had geodesic error below 0.1 for S-MDS approach while for our method above 98% of correspondences fell below the 0.1 geodesic error. Another example from the "all shapes" table shows 100% of sample points had geodesic error below 0.15 for our approach when compared against 95% for S-MDS. We also generated a graphical representation of the data, where x-axis depicts geodesic error threshold, τ, and y-axis is the average percentage of point correspondence that fall below the threshold τ. The top left, top right and bottom left graphs in Figure 2 are graphical representation of Table 1. Clearly, we can see that the result of our method outperforms that of spectral-MDS.

Overall our algorithm produces better results when matching human shapes. Bottom right of Figure 2 is a representation of the percentage of correspondence measure of all six animal shapes of the TOSCA database.

As the idea of multidimensional scaling is to find a rigid alignment of the embedded image of the shapes, in the next experiment, we used the Iterative Closest Point (ICP) algorithm to compute such alignment. Figure 3 is a picture of two near-isometric wolf shapes before and after computing their ICP alignment. We also performed a comprehensive experiment on shapes from the SPACE database. In this experiment, we selected the first 50 eigenfunctions for our spectral interpolation. We randomly selected a model and matched with several probes. Having computed the canonical forms, we computed the rigid alignment between the canonical form images of the matching, and next we used a relative straight forward scheme to find the similarity measure between them. First, we transformed the matrix of the output of the canonical form S and T into a vector s and t. And then given a range of threshold, the dis(similarity) between them by function $(s\cdot t)/norm(s)\cdot norm(t)$ is computed, where "." is the inner product between two vectors and $norm(\ )$ is the Euclidean norm of the vector. The

range of threshold is between 0 and 1 such that the closer the function is to 1 the more similar S and T are, conversely, the closer the function is to 0 the more dissimilar S and T are. The results from 10 similarity measures were sampled from our experiment as shown in Table 2. Experimental results from the table show an improvement in our similarities measure when compared with that of the spectral multidimensional scaling.

7 CONCLUSIONS

In this paper we argued that approaching the novel method of spectral multidimensional scaling with a

theoretical sound distance operator in biharmonic distance proves to further reduce the topological complexities of the embeddings. Taking advantage of the global shape awareness property of the biharmonic distance operator, we were able to get a minimal distorted canonical form thus making the computing of a rigid assignment of canonical forms more efficient and accurate. Experimental results show a comparable and even better result to a state-of-the-art method. Future prospect of this study might include using other distance operators to compute the dimension reduction problem that might achieve a more favorable result.
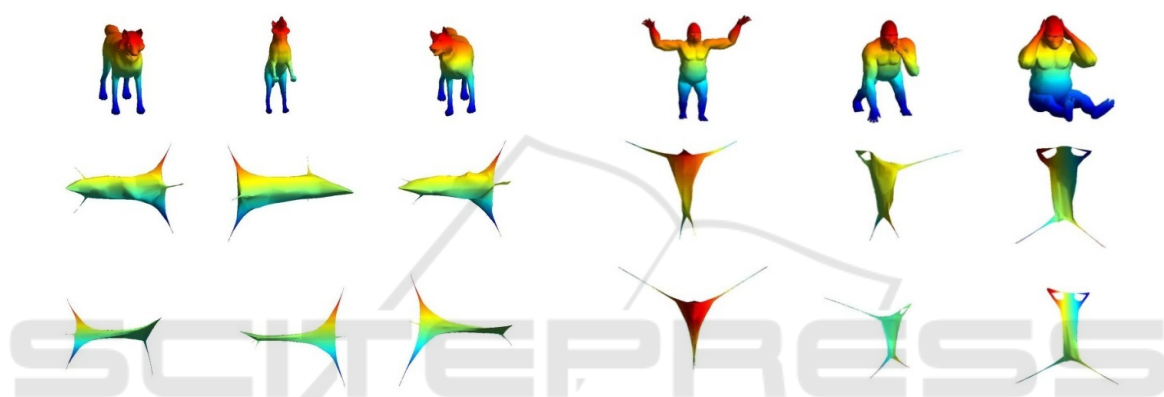
Figure 1: Embedding of wolf and gorilla shapes into canonical forms. From top to bottom depicts original shape, followed by canonical form obtained by Spectral MDS, Spectral MDS using biharmonic distance.

Table 1: Shows the data of varying geodesic error threshold D, between the model and probe against the average percentage of point correspondence.

Geodesic error(D)	Animal Shapes		Human Shapes		All Shapes	
	S-MDS Pts.(%)	SMDS-Biharmonic Pts. (%)	S-MDS Pts. (%)	SMDS-Biharmonic Pts. (%)	S-MDS Pts. (%)	SMDS-Biharmonic Pts. (%)
0	1.1183	1.3707	1.2298	1.2207	1.2413	1.3524
0.0125	4.4088	6.7875	4.452	7.3923	4.8266	7.1525
0.025	12.1579	19.1776	14.7096	20.9908	14.596	19.9216
0.0375	24.7667	40.4431	31.5826	46.061	30.4995	43.1803
0.05	39.3009	63.3398	51.1159	66.3549	48.8439	65.2796
0.0625	49.7646	81.8704	68.9267	81.5946	63.7864	82.0446
0.075	57.1189	91.3908	83.3491	92.5794	75.1602	92.2939
0.0875	62.7122	96.8784	90.7177	97.5841	81.9415	97.3656
0.1	67.3756	98.8709	94.6324	99.2309	86.438	99.0808
0.1125	71.5725	99.6609	98.0789	99.7937	90.1884	99.7827
0.125	76.0111	99.9399	99.2249	99.8841	93.1298	99.9328
0.1375	78.8878	99.9553	99.6353	99.9521	94.6593	99.9761
0.15	81.1456	99.9702	99.7597	100	95.6654	100
0.1625	83.5624	99.9702	99.881	100	96.7655	100
0.175	85.7585	100	99.9575	100	97.6749	100
0.1875	87.1764	100	99.9745	100	98.1592	100
0.2	89.0674	100	99.9915	100	98.8559	100
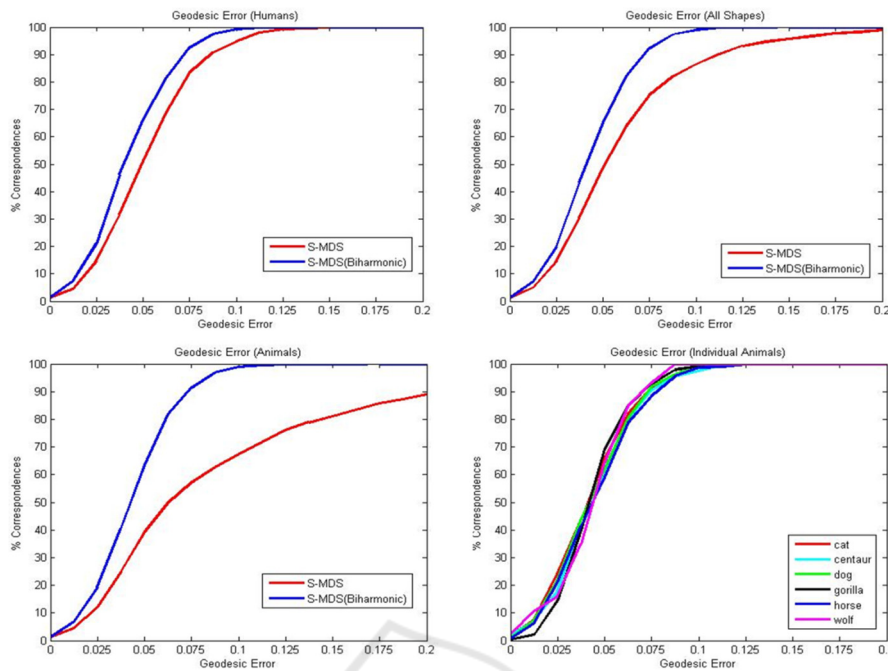
Figure 2: Graphical representation evaluating the geodesic error of correspondence between different categories of shapes. All graphs show percentage of correspondence between the thresholds of a normalized geodesics error(0-0.2). Top left, top right and bottom left show comparison of the correspondence between regular S-MDS and S-MDS using biharmonic distance. Bottom right shows the percentage of correspondence between six different shapes using S-MDS using biharmonic distance.
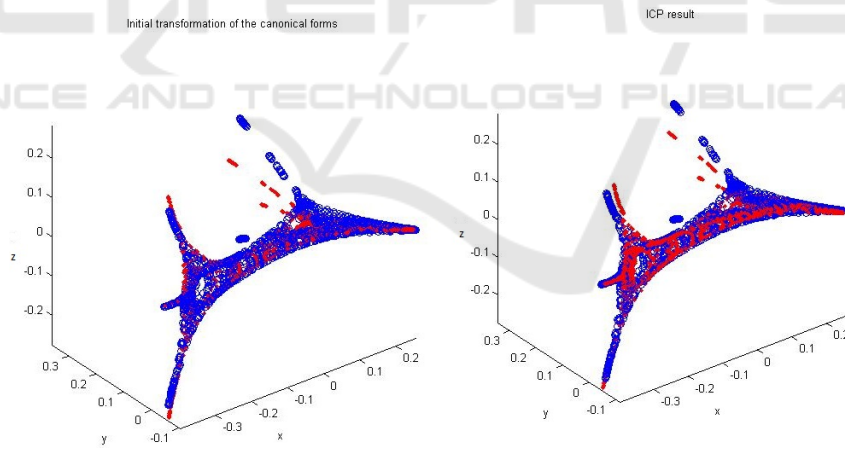
Figure 3: An alignment of canonical forms using Iterative Closest Point (ICP) algorithm. From left to right are images of pre-alignment and post-alignment of two wolf shapes.

Table 2: Comparison of similarity measure function. A model is compared against ten probes with a threshold between 0 and 1. The closer the value to 1 the more similar the model and probe are.

Shape Similarity Measure	
Spectral MDS	Spectral MDS-Biharmonic
0.9034	0.9117
0.8761	0.8828
0.8720	0.8813

0.8398	0.8505
0.8840	0.8928
0.8565	0.8653
0.7255	0.7282
0.8746	0.8851
0.8987	0.9045
0.8741	0.8821

ACKNOWLEDGEMENTS

REFERENCES

Vankaick, O., Zhang, H., Hamarneh, G., Cohen-Or, D., 2011. A survey on shape correspondence, *Computer Graphics Forum*, 30(6): 1681-1707.

Sumner, R. W., Popovic, J., 2004. Deformation transfer for triangle meshes, *ACM Transactions on Graphics*, 23(3): 399-405.

Kreavoy, V., Sheffer, A., Gotsman, C., 2003. Matchmaker: constructing constrained texture maps, *ACM Transaction on Graphics,* 22(3): 326-333.

Alexa, M., 2002. Recent advances in mesh morphing, *Computer Graphics Forum*, 21(2): 173-198.

Jain, A., Zhang, H., 2006. Shape-based retrieval of articulated 3D models using spectral embeddings, In *Proc. of Geometric Modeling and Processing*, SPRINGER: 295-308.

Bronstein, A. M., Bronstein, M. M., Kimmel, R., 2006. Generalized multidimensional scaling: a framework for isometry-invariant partial surface matching, In *Proceedings of the National Academy of Sciences of the United States of America*, 103(5): 1168-1172.

Schwartz, E. L., Shaw, A., Wolfson, E., 1989. A numerical solution to the generalized mapmaker's problem: flattening non convex polyhedral surfaces, *IEEE Transactions on Pattern Analysis and Machine Intelligence*, 11(9): 1005-1008.

Zigelman, G., Kimmel, R., Kiryati, N., 2002. *IEEE Transactions on Visualization and Computer Graphics,* 8(2): 198-207.

Elad, A., Kimmel, R., 2003. On bending invariant signatures for surfaces, *IEEE Transactions on Pattern Analysis and Machine Intelligence*, 25(10): 1285-1295.

Gromov, M., 1981. Structures metriques pour les varietes riemanniennes, *Textes Mathe´ matiques*, 1.

Wolter, F., Reuter, M., Peinecke, N., 2006. Laplace-Beltrami spectra as 'shape-DNA' of surfaces and solids, *Computer-Aided Design*, 38(4): 342-366.

Jain, V., Zhang, H., VanKaick, O., 2011. Non-rigid spectral correspondence of triangle meshes, *International Journal on Shape Modeling*, 13(1): 101-124.

Kim, V., Lipman, Y., Funkhouser, T., 2011. Blended intrinsic maps, *ACM Transactions on Graphics*, 30(4): 76-79.

Ovsjanikov, M., Chen, M. B., Solomon, J., Butscher, A., Guibas, L., 2012. Functional maps: a flexible representation of maps between shapes, *ACM Transactions on Graphics*, 31(4): 1-11.

Rustamov, R., 2007. Laplace-Beltrami eigenfunctions for deformation invariant shape representation, In *Symposium on Geometry Processing*, SPRINGER: 225-23.

Coifman, R., Lafon, S., 2006. Diffusion maps, *Applied and Computional Harmonic Analysis*, 21(1): 5-30.

Sun, J., Ovsjanikov, M., Guibas, L. J., 2009. A concise and provably informative multi-scale signature based on heat diffusion, *Computer Graphics Forum*, 28(5): 1383-1392.

Aubry, M., Schlickewei, U., Cremers, D., 2011. The wave kernel signature: a quantum mechanical approach to shape analysis, In *Proceedings of the 2011 IEEE Conference on Computer Vision Workshops*, IEEE: 1626-1633.

Aflalo, Y., Kimmel, R., 2013. Spectral multidimensional scaling, In *Proceedings of National Academy of Sciences*, IEEE: 18052-18057.

Lipman, Y., Rustamov, R., Funkhouser, T., 2010. Biharmonic distance, *ACM Transactions on Graphics*, 29(3): 27.

Fouss, F., Pirotte, A., Renders, J., Saerens, M., 2007. Random-walk computation of similarities between nodes of a graph with application to collaborative recommendation, *IEEE Transactions on Knowledge and Data Engineering*, 19(3): 355-369.

Yen, L., Fouss, F., Deacaestecjer, C., Francq, P., Saerens, M., 2007. Graph nodes clustering based on the commute-time kernel, In *Proceeding of 11th Pacific-Asia Conference on Knowledge Discovery and Data Mining*, SPRINGER: 1037-1045.

Grinspun, E., Gingold, Y., Reisman, J., Zorin, D., 2006. Computing discrete shape operators on general meshes, *Computer Graphics Forum*, 25(3): 547–556.

Meyer, M., Desbrun, M., Schrder, P., Barr, A. H., 2003. Discrete differential-geometry operators for triangulated 2-manifolds, In *Visualization and Mathematics III*, SPRINGER: 35-57.

Bronstein, A. M., Bronstein, M. M., Kimmel, R., 2009. *Numerical geometry of non-rigid shapes*, Springer, New York, 1st edition.

Anguelov, D., Srinivasan, P., Pang, H. C., Koller, D., Thrun, S., Davis, J., 2004. The correlated correspondence algorithm for unsupervised registration of non-rigid surfaces, In *Proceeding of Conference on Neural Information Processing Systems*, MIT PRESS: 33-40.